JOURNAL OF COMPUTATIONAL PHYSICS 14, 200–222 (1974)

Reduction of the Grid Effects in Simulation Plasmas*

LIU CHEN,† A. BRUCE LANGDON,‡ AND C. K. BIRDSALL

Department of Electrical Engineering and Computer Sciences, and Electronics Research Laboratory, University of California, Berkeley, California 94720

Received July 3, 1973

The electromagnetic field grids in fine-resolution two-dimensional or medium-resolution three-dimensional plasma simulation are very large. We propose a method whereby only a fraction of the grid need be in fast core at any given time. The basic idea is to do several consecutive field solutions with coarse grids displaced relative to one another. The separate solutions may pertain to different time steps ("jiggling") or the same time step ("interlacing"). The combination of these separate solutions can provide some aspects of the accuracy improvement obtainable with the fine grid which is the superposition of the separate grids. These techniques may be useful when one is strongly limited by the size of random-access memory but can afford to place greater demands on serial-access memory and processor speed. Their effect is to reduce "aliasing" errors, in which plasma perturbations are unphysically coupled when their wave numbers differ by wave vectors characteristic of the grid. Resolution may then be improved by methods described elsewhere. In order to evaluate these methods quantitatively, dispersion relations for plasma oscillations are examined. Aliasing effects, such as grid-induced instability, can be greatly reduced. However, depending on the smoothness of the velocity distribution, "jiggling" can introduce new troublesome modes with frequencies $\sim \Delta t^{-1}$; "interlacing" has no known ill side effects. Simulation results are in agreement with theory. In two and three dimensions, there is also a decrease in computation time compared to using a finer gride with similar reduction in grid effects.

1. INTRODUCTION

Recently, the existence of nonphysical grid effects was both predicted for and observed in computer plasma simulations [1–5]. These grid effects are introduced because the field quantities (e.g., electric field, potential, and charge density in a normal electrostatic code) are known only at the grid points, producing an artificial periodicity. Consequently, in addition to the plasma waves, one has the nonphysical grid alias waves [1–3]. Another viewpoint is that the interparticle force

* Research supported by Atomic Energy Commission Grant AT04 334 PA 128.

† Present address: Bell Laboratories, Murray Hill, NJ 07974.

‡ Permanent address: Lawrence Livermore Laboratory, Livermore, CA.

depends not only on the separation of the particles but also on their placement relative to the grid [2]. These alias waves not only cause errors in field calculations [6] but also can seriously alter the stability of the simulation plasmas [1–3] and increase the noise [3, 4].

Generally, the grid effects are stronger for a smaller ratio of Debye length to grid spacing, $\lambda_D/\Delta x$; for example, a Maxwellian plasma (physically stable) with $\lambda_D = 0.1\,\Delta x$ and NGP interpolation is found to be unstable computationally, with a maximum growth rate of $0.1\omega_p$ [2]. This could well discourage simulations of higher dimensions (2 and 3 dimensions). This is because in higher-dimensional simulations; one has to live with coarse grids due to the size limit of the random-access memory, e.g., a $64 \times 64 \times 64$ grid or a 512×512 grid is an array of length 262, 144 for *each* electric field component. Yet, in order to observe collective phenomena, the system must be many λ_D's across. Therefore, in higher-dimensional simulations, $\lambda_D/\Delta x$ will tend to be small ($\sim 10^{-1}$) and the nonphysical grid instabilities can seriously distort the desired physics.

Two schemes have been proposed to allow use of coarse grids and at the same time reduce these nonphysical grid effects. One is called "grid jiggling"; that is, at each time step the grid is displaced from the preceding grid. The grid can be jiggled either randomly or orderly. The code is otherwise the usual algorithm (e.g., see [7]). The other scheme, "grid interlacing", is to use several of these displaced grids at the *same* time step. Fields are calculated on each grid and a modified leapfrog particle-pushing scheme is used. A sketch of these grid-moving schemes is shown in Fig. 1. The basic idea underlying these two schemes is to eliminate or, at least, reduce the coherent feedback of the most troublesome aliases.

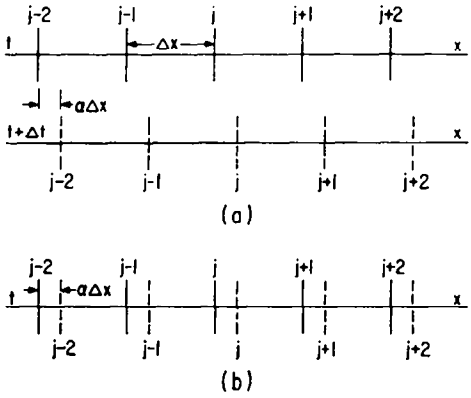

FIG. 1. Sketch to illustrate grid-jiggling and interlacing (a) two-time-step jiggled grids and (b) two interlaced grids. $0 \leqslant \alpha \leqslant 1$.

In the following sections, the two schemes are examined analytically and computationally. Ions are immobile and serve as a neutralizing background. Electrons have a uniform zero-order charge density. Theories of grid jiggling and grid interlacing are presented in Sections 2 and 3, respectively. Dispersion relations for certain cases are derived and numerically evaluated. Section 4 presents experimental verifications of the theories. In Section 5 is an experiment with randomly jiggled grid, which cannot be analytically treated. In Section 6 we present a theoretical study of two-dimensional simulations with diagonally jiggled or interlaced grids. The final conclusions and discussions are in Section 7.

2. Theory of Simulations with Jiggled Grids

In this section we derive the linear dispersion relations for simulation with jiggled grids in order to check the grid effects on the stability of simulation plasmas. First, we consider a special case of grid jiggling, i.e., the equal-spacing case. This special case is interesting because (1) it is easy to implement in actual simulation and (2) the corresponding dispersion relation can be readily obtained. The more involved theory of the general case is presented in the Appendix.

Let us assume that a jiggling cycle consists of N time steps. Here $N \geqslant 1$ is an integer. With equal-spacing grid jiggling, the position of the jth grid, x_j, at the ℓth time step then is

$$x_j(\ell\, \Delta t) = x_j[(KN + s)\, \Delta t] = (j + s/N)\, \Delta x,$$

where $0 \leqslant K =$ integers $< \infty$ and $s = 0, 1, \ldots, N - 1$. A useful viewpoint is that the grids are moving at a constant velocity, $\Delta x/N\, \Delta t \hat{x}$. If the grids were fixed as in normal simulation codes, the linear dispersion relation would be [3]

$$\epsilon_0(k, \omega) = 1 + \omega_{pe}^2 \frac{\kappa}{K^2} \sum_p |S(k_p)|^2 \int dv f_0' \frac{\Delta t}{2} \cdot \cot(\omega - k_p v) \frac{\Delta t}{2}, \qquad \operatorname{Im} \omega \geqslant 0. \tag{1}$$

Here Langdon's notation is followed. ω_{pe} is the electron plasma frequency; f_0 is the electron initial velocity distribution; $A(k, \omega)$ is the spatial-Fourier and time-Laplace transforms of $A(x, t)$; $k_p = k - pk_g$ and $k_g = 2\pi/\Delta x$. S is the effective shape factor. For NGP, $S(k) = \sin \frac{1}{2}k\, \Delta x/\frac{1}{2}k\, \Delta x$. For CIC with cell-size clouds, $S(k) = (\sin \frac{1}{2}k\, \Delta x/\frac{1}{2}k\, \Delta x)^2$. For the normal three-point Poisson's equation, $\kappa(k)/K^2(k) = \Delta x/2 \tan(k\, \Delta x/2)$. With the grids moving, the aliases ($p \neq 0$) experience additional doppler shifts. The amount of doppler shift for the pth alias in this case is $pk_g\, \Delta x/N\, \Delta t = 2\pi p/N\, \Delta t$. Thus, replacing ω in (1) by $\omega - 2\pi p/N\, \Delta t$,

we obtain the dispersion relation for the N-time-step equal-spacing jiggling case, which is[1]

$$\epsilon_N(k, \omega) = 1 + \omega_{pe}^2 \frac{\kappa}{K^2} \sum_p |S(k_p)|^2 \int dv f_o' \frac{\Delta t}{2} \cdot \cot\left[-\frac{p\pi}{N} + (\omega - k_p v)\frac{\Delta t}{2}\right] = 0,$$

$$\text{Im } \omega \geqslant 0. \quad (2)$$

We will examine the properties of (2) corresponding to $N = 2$ and 3, since they are most likely to be used in simulations.

For $N = 2$, (2) can be written as

$$\epsilon_2(k, \omega) = 1 + \omega_{pe}^2 \frac{\kappa}{K^2} \left\{ \sum_{p=\text{even}} |S(k_p)|^2 \int dv f_o' \frac{\Delta t}{2} \cdot \cot(\omega - k_p v)\frac{\Delta t}{2} \right.$$

$$\left. - \sum_{p=\text{odd}} |S(k_p)|^2 \int dv f_o' \frac{\Delta t}{2} \cdot \tan(\omega - k_p v)\frac{\Delta t}{2} \right\} = 0, \quad \text{Im } \omega \geqslant 0. \quad (3)$$

For $|(\omega - k_p v)(\Delta t/2)| \ll 1$, (3) approximates as

$$\epsilon_2(k, \omega) \cong 1 + \omega_{pe}^2 \frac{\kappa}{K^2} \sum_{p=\text{even}} |S(k_p)|^2 \int dv f_o' \frac{1}{\omega - k_p v}$$

$$- \left(\frac{\omega_{pe}\Delta t}{2}\right)^2 \frac{\kappa}{K^2} \sum_{p=\text{odd}} |S(k_p)|^2 k_p \cong 0, \qquad \text{Im } \omega \geqslant 0. \quad (4)$$

(4) indicates that odd aliases will affect the dispersion to order $(\omega_{pe}\Delta t)^2$ only. Most important of all is that they have no dependence on ω and the terms are real; thus they contribute only to the real part of ω. That is to say, instabilities or damping due to odd aliases will be suppressed if one jiggles the grids fast enough such that $|(\omega - k_p v)(\Delta t/2)| \ll 1$. The condition $|(\omega - k_p v)(\Delta t/2)| \ll 1$ can be violated by higher p terms and higher ω's. The presence of $|S(k_p)|^2$, however, significantly reduces the influence of higher p terms. Higher ω's must be considered. Since $\epsilon_2(k, \omega + (2\pi/\Delta t)) = \epsilon_2(k, \omega)$, only frequencies around $\pi/\Delta t$ (the jiggling frequency) need to be investigated. Let $\omega = \omega' + \pi/\Delta t$. Then

$$\epsilon_2\left(k, \omega' + \frac{\pi}{\Delta t}\right) = 1 + \omega_{pe}^2 \frac{\kappa}{K^2} \left\{ \sum_{p=\text{odd}} |S(k_p)|^2 \int dv f_o' \frac{\Delta t}{2} \cdot \cot(\omega' - k_p v)\frac{\Delta t}{2} \right.$$

$$\left. - \sum_{p=\text{even}} |S(k_p)|^2 \int dv f_o' \frac{\Delta t}{2} \cdot \tan(\omega' - k_p v)\frac{\Delta t}{2} \right\} = 0,$$

$$\text{Im } \omega \geqslant 0. \quad (5)$$

[1] Since f_o is a general expression, the following analyses are also applicable when the plasma undergoes bulk motion.

For $|(\omega' - k_p v)(\Delta t/2)| \ll 1$, the dispersion relation approximates as

$$\epsilon_2(k, \omega) \cong 1 + \omega_{pe}^2 \frac{\kappa}{K^2} \sum_{p=\text{odd}} |S(k_p)|^2 \int dv f_o' \frac{1}{\omega' - k_p v} - \left(\frac{\omega_{pe}\Delta t}{2}\right)^2 \frac{\kappa}{K^2} \sum_{p=\text{even}} |S(k_p)|^2 k_p \cong 0, \qquad \text{Im}\,\omega' \geqslant 0. \quad (6)$$

Thus, for frequencies around $\pi/\Delta t$, the roles of even and odd aliases are interchanged, i.e., the odd aliases contribute much more significantly than the even aliases.

For the case of a cold drifting electron beam with $v_{\text{drift}} = 0.12\omega_{pe}\Delta x$ and $k\Delta x = \pi/4$, numerical evaluation in the $\Delta t \to 0$ limit for the fixed-grids CIC case indicates a nonphysical instability with a maximum growth rate $\omega_i = 0.04\omega_{pe}$ at $\omega_r = .8\omega_{pe}$. In the jiggling case, (4) gives maximum growth rate, $\omega_i = .02\omega_{pe}$ at $\omega_r = 1.4\omega_{pe}$. (6), however, gives a maximum growth rate, $\omega_i = .05\omega_{pe}$ at $\omega_r = (\pi/\Delta t) + .65\omega_{pe}$. Thus, in this case, jiggling the grids has has two effects; one is that for $|\omega\,\Delta t| \ll 1$, it reduces the nonphysical instabilities; the other is that it creates new unstable modes with $\omega_r \sim \pi/\Delta t$.

This has been checked in computer simulations to be discussed in Section 4. The cold drifting case is pathologically unstable and is discussed as a check on the theory.

The effects of grid jiggling on the more interesting Maxwellian plasmas have also been investigated numerically through (4) and (6). In the case of (6), Nyquist diagrams were drawn to check the stability. For $\lambda_D = 0.1\,\Delta x$, the high frequency ($\omega_r \sim \pi/\Delta t$) mode has been found to be stable over the range of $k\,\Delta x$ investigated; $k\,\Delta x = \pi/8$ to $\pi/2$. Thus, only even aliases contribute the grid instabilities at low frequencies and, expectedly, the growth rates are greatly reduced. For example, with $k\,\Delta x = \pi/4$, the growth rate is reduced from $1.2 \times 10^{-3}\omega_{pe}$ of fixed grids to $3 \times 10^{-5}\omega_{pe}$ for jiggled grids. A more complete comparison of growth rates is shown in Fig. 2.

For $N = 3$, (2) reduces to

$$\epsilon_3(k, \omega) = 1 + \omega_{pe}^2 \frac{\kappa}{K^2} \sum_{p=3q} |S(k_p)|^2 \int dv f_o' \frac{\Delta t}{2} \cot(\omega - k_p v) \frac{\Delta t}{2} + \omega_{pe}^2 \frac{\kappa}{K^2} \sum_{p=3q+1} |S(k_p)|^2 \int dv f_o' \frac{\Delta t}{2} \cot\left[-\frac{\pi}{3} + (\omega - k_p v)\frac{\Delta t}{2}\right] + \omega_{pe} \frac{\kappa}{K^2} \sum_{p=3q+2} |S(k_p)|^2 \int dv f_o' \frac{\Delta t}{2} \cot\left[\frac{\pi}{3} + (\omega - k_p v)\frac{\Delta t}{2}\right] = 0,$$

$$q = \text{integers}, \qquad \text{Im}\,\omega \geqslant 0. \quad (7)$$

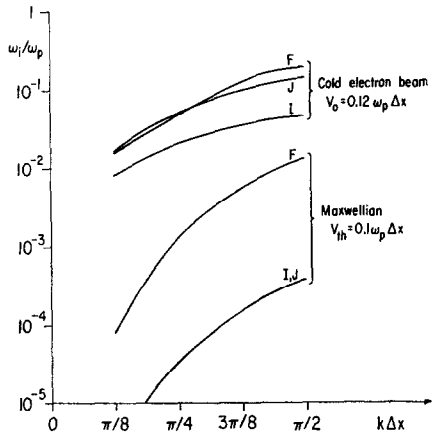

FIG. 2. Plots of the growth rates for the cold electron beam and a Maxwellian plasma with $k\Delta x$ from $\pi/8$ to $\pi/2$. *F*, *J*, and *I* denote fixed, two-time-step equal-spacing jiggled, and two equal-spacing interlaced grids, respectively. CIC is assumed.

Assuming $|(\omega - k_p v)(\Delta t/2)| \ll 1$, one has

$$\epsilon_3(k, \omega) \cong 1 + \omega_{pe}^2 \frac{\kappa}{K^2} \sum_{p=3q} |S(k_p)|^2 \int dv f_0' \frac{1}{\omega - k_p v} - \left(\frac{\omega_{pe}\Delta t}{2 \sin \pi/3}\right)^2 \frac{\kappa}{K^2} \sum_{p\neq 3q} |S(k_p)|^2 k_p \cong 0, \quad q = \text{integers}, \quad \text{Im}\,\omega \geqslant 0. \tag{8}$$

Therefore, only aliases with their alias numbers, p, equal to multiples of three contribute significantly to $\epsilon_3(k, \omega)$. Furthermore, other aliases only affect the real part of ω to order of $(\omega_{pe}\Delta t)^2$ and, hence, will not cause any nonphysical instability or damping. As in the two-time-step jiggling case, high-frequency modes may be introduced. It is obvious from (7) that for $\omega_r \simeq 2\pi/3\,\Delta t$, aliases with $p = 3q + 1$ will play the dominant role. Similarly for $\omega_r \simeq 4\pi/3\,\Delta t$, aliases with $p = 3q + 2$ are dominant.

In summary, the results presented in this section indicate that grid jiggling shifts certain aliases (e.g., odd aliases in the two-time-step equal-spacing jiggling case) to frequencies comparable to the jiggling frequency. These shifted aliases *sometimes* can still create strong nonphysical grid instabilities. One, therefore, would like to have those notorious aliases completely eliminated. In the next section an algorithm, grid interlacing, is proposed to achieve this purpose, and the corresponding theoretical analyses indicate that it indeed does.

3. Theory of Simulations with Interlaced Grids

The one-dimensional, two-interlaced-grids case is analyzed here to illustrate the approaches to more general cases. Grid system 2 is displaced from grid system 1 by $\alpha\,\Delta x$, $0 \leqslant \alpha \leqslant 1$. That is, the position of jth grid, x_j, is at $j\,\Delta x$ in grid system 1 and $(j+\alpha)\,\Delta x$ in grid system 2. Figure 1(b) is a sketch of the two interlaced grid systems. Subscripts 1 and 2 are used to denote quantities associated with these two grid systems.

A suggested algorithm is that given particle density at t, $n(x_t)$, grid charge density and electric field are first calculated on system 1. This electric field, weighted to produce the force, is used to move $v_{t-\Delta t/2}$ to an intermediate velocity, v', without changing the x_t. The same $n(x_t)$ is then used with the same charge-sharing scheme to obtain grid charge density and electric field on system 2. Force on the particle is calculated from this electric field using the same field-weighting scheme. This force is then used to calculate $v_{t+(1/2)\Delta t}$ from the intermediate v'. With $v_{t+\Delta t/2}$ obtained, x_t are moved to $x_{t+\Delta t}$. The scheme works in the following way:

First:

$$n(x_t) \to \rho_{1,t}(x_j) \to E_{1,t}(x_j) \to F_1(x_t),$$
$$v' = v_{t-\Delta t/2} + (F_1/m)\,\Delta t/2;$$

then, using grid system 2,

$$\begin{aligned} n(x_t) &\to \rho_{2,t}(x_j) \to E_{2,t}(x_j) \to F_2(x_t), \\ v_{t+\Delta t/2} &= v' + (F_2/m)\,\Delta t/2, \\ x_{t+\Delta t} &= x_t + \Delta t \cdot v_{t+\Delta t/2}, \end{aligned} \tag{9}$$

or written in an equivalent form,

$$\begin{aligned} n(x_t) &\begin{cases} \to \rho_{1,t}(x_j) \to E_{1,t}(x_j) \to F_1(x_t), \\ \to \rho_{2,t}(x_j) \to E_{2,t}(x_j) \to F_2(x_t), \end{cases} \\ v_{t+\Delta t/2} &= v_{t-\Delta t/2} + (\Delta t/2m)(F_1 + F_2), \\ x_{t+\Delta t} &= x_t + \Delta t\, v_{t+\Delta t/2}. \end{aligned} \tag{9'}$$

Thus, one has an effective force $(F_1 + F_2)/2$ and the corresponding dispersion relation is

$$\epsilon_I(k,\omega) = 1 + \omega_{pe}^2 \frac{\kappa}{K^2} \sum_p |S(k_p)|^2 \left(\frac{1 + e^{i2\pi p\alpha}}{2}\right) \int dv f_o' \frac{\Delta t}{2} \cot\left[(\omega - k_p v)\frac{\Delta t}{2}\right] = 0,$$

$$\operatorname{Im}\omega \geqslant 0. \tag{10}$$

Generally, the result is rather involved and only special cases, $\alpha = 0$, 1, and 1/2, will be considered here.

(a) $\alpha = 0$, 1 (no interlacing). The dispersion relation for fixed grids, (1), is recovered as it should be.

(b) $\alpha = 1/2$, (10) becomes

$$\epsilon_{2,I}(k, \omega) = 1 + \omega_{pe}^2 \frac{\kappa}{K^2} \sum_{p=\text{even}} |S(k_p)|^2 \int dv f_o' \frac{\Delta t}{2} \cot\left[(\omega - k_p v)\frac{\Delta t}{2}\right] = 0, \quad \text{Im}\,\omega \geqslant 0. \quad (11)$$

It is obvious from (11) that interlacing the grids completely eliminates the odd aliases. Thus, the growth rates of the nonphysical grid instabilities can be reduced without introducing new modes.

For example, in the cold drifting electron beam case with $v_{\text{drift}} = 0.12\omega_p \Delta x$ and $k \Delta x = \pi/4$, the growth rate is reduced from $4.5 \times 10^{-2}\omega_p$ to $2. \times 10^{-2}\omega_p$. For a thermal Maxwellian plasma with $v_{\text{th}} = 0.1\omega_p \Delta x$ and $k \Delta x = 3\pi/8$, the growth rate is reduced from $5.3 \times 10^{-3}\omega_p$ to $1.1 \times 10^{-4}\omega_p$. Figure 2 shows the growth rates corresponding to the three ways of moving the grids. Since the jiggling modes are stable in the Maxwellian plasma considered here, so far as instability is concerned, there is no difference between grid jiggling and grid interlacing.

It is straightforward to extend the particle-moving scheme as well as the theory to simulations with N equal-spacing interlaced grids. The corresponding dispersion relation then is

$$\epsilon_{N,I}(k, \omega) = 1 + \omega_{pe}^2 \frac{\kappa}{K^2} \sum_{p=JN} |S(k_p)|^2 \int dv f_o' \frac{\Delta t}{2} \cdot \cot(\omega - k_p v)\frac{\Delta t}{2} = 0, \quad J = \text{integers}, \quad \text{Im}\,\omega \geqslant 0. \quad (12)$$

4. Experimental Verifications

The cold drifting electron beam case is used to verify the theories. Three computer experiments are done with the grids fixed, jiggled, and interlaced, respectively. The simulation model is one dimensional, electrostatic, and periodic. Ions are immobile and the CIC method is used. The experimental parameters are

System length, $L = 16 \Delta x$; $\omega_{pe} \Delta t = 0.157$;
Drifting velocity, $v_o = 0.12\omega_{pe} \Delta x$;
Number of electrons, $N = 3200$;
Excited wave number, $k_o \Delta x = 3\pi/8$.

All electrons with $v = v_o$ are uniformly spaced between 0 and L. The initial excitation is $v(x, t = 0) = v_o(1 + 0.002 \cos k_o x)$. Since comparison with the linear theory is the main concern, only k_o is kept in the simulations. This technique suppresses the higher spatial modes which tend to occur in the nonlinear stage.

(a) *Fixed Grids.* Numerical evaluation of the corresponding dispersion relation indicates that the simulation plasma is nonphysically unstable and the most unstable mode has $\omega_i = 0.14\omega_{pe}$. Figure 3 shows the plots of the various energies normalized to the initial kinetic energy. The growth rate measured from the field-energy plot is in good agreement with the theoretical value. Since the instability is of traveling wave nature, the oscillation frequency, ω_r, cannot be obtained from the field-energy plot. To measure ω_r, the plot of the square of the cosine component of the electric field (hereafter called cosine-square plot) is shown in Fig. 3(d). In

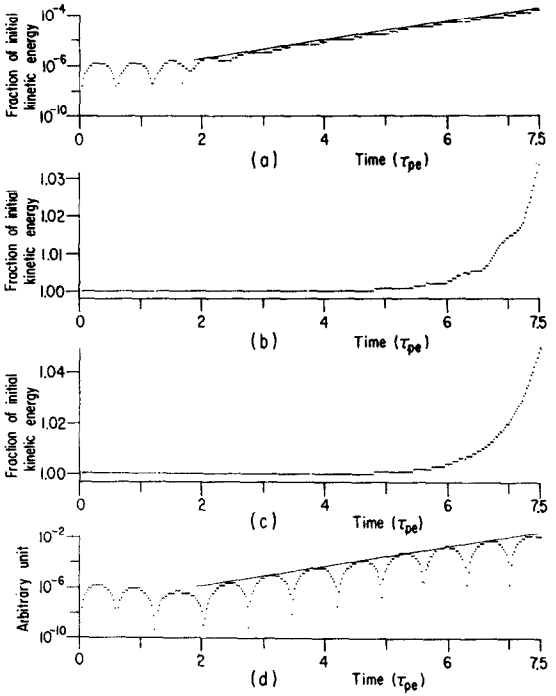

FIG. 3. Experiment of cold drifting beam with $v_o = 0.12\ \omega_{pe}\ \Delta x$ and fixed grids. Plots of (a) electric field energy, (b) kinetic energy, (c) total energy, and (d) square of the cosine component of the electric field vs time. Energies are normalized with respect to initial kinetic energy. τ_{pe} is the electron plasma period. The lines added to (a) and (d) are best fits to the data; their slopes (accurate to a few percent) agree with the predicted growth rates. (This same comment applies to the lines added to the results shown in Figs. 4–6.)

this plot, both ω_r and ω_i are measured. The results agree with the theory. Okuda [5] and Langdon [8] also did some experiments with cold drifting electron beam and had similar results.

(b) *Jiggled Grids.* In this experiment, the position of the jth grid is $j\,\Delta x$ at even time steps and $(j + 1/2)\,\Delta x$ at odd time steps. The rest of the simulation scheme is the same as that with the grids fixed. Numerical evaluations of the corresponding dispersion relation indicate that the most unstable mode is produced by the odd aliases and has $\omega_r = (\pi/\Delta t) - 0.6\omega_{pe}$ and $\omega_i = 0.09\omega_{pe}$. If such an instability does exist, then some care is needed to measure it. Since $\omega_r\,\Delta t \cong \pi$, such a mode has opposite signs between two neighboring time steps, and due to the presence of other excited modes, all the physical quantities are expected show odd–even "jumping".

Soon after the initiation of the experiment, odd–even jumpings were observed, indicating the existence of a $\omega_r \cong \pi/\Delta t$ mode. Figure 4 shows the normalized

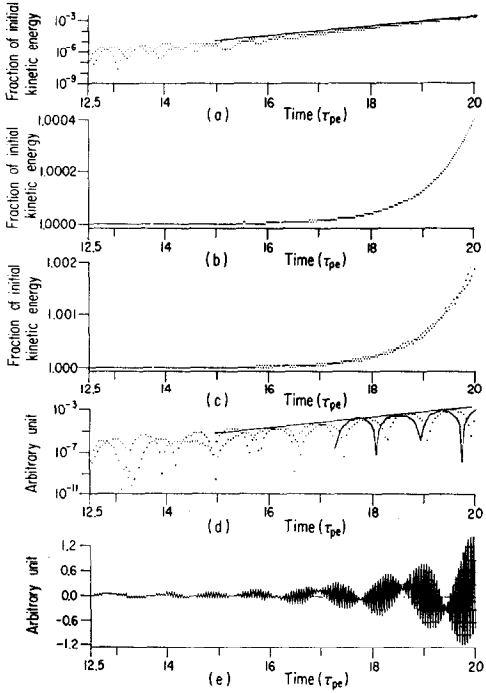

FIG. 4. Experiment of cold drifting beam with $v_o = 0.12\,\omega_{pe}\,\Delta x$ and two-time-step equal-spacing grid jiggling. Plots of (a) electric field energy, (b) kinetic energy, (c) total energy, (d) square of the cosine component of the electric field, and (e) the sine component of the electric field vs time.

energies and the cosine square in the later stage ($t \geqslant 12.5\tau_{pe}$) where the nonphysical instability is clearly demonstrated. Figure 4(e) is the plot of the sine component (*not squared*) of the electric field versus time. It is then obvious that the instability has $\omega_r \cong \pi/\Delta t$. To measure ω_i and $\omega_r - \pi/\Delta t$, the nuisance of odd–even jumping can be avoided by making measurements *only* at either even or odd time steps. The growth rate measured from the field-energy plot agrees with the theoretical value, $0.09\omega_{pe}$. Both $\omega_r - \pi/\Delta t$ and ω_i are measured from the cosine-square plot and are in good agreement with the theory.

(c) *Interlaced Grids.* Two interlaced grid systems were used in this experiment. One has its jth grid at $j\,\Delta x$, the other at $(j + 1/2)\,\Delta x$. The simulation scheme is described in Section 3. According to the theory, only even aliases contribute to the nonphysical properties of the simulation plasma, and numerical evaluations find that the most unstable mode has $\omega_r = -1.4\omega_{pe}$ and $\omega_i = 0.03\omega_{pe}$.

We did two experiments on this case with different schemes of initial excitation. In the first experiment, we used the usual initial-velocity modulation. Since the growth rate is small, the instability took a long time to emerge. Only after $t \cong 25\tau_{pe}$ did it became the dominant mode and the measurement of the growth rate is not very satisfactory. We then did another experiment using initial-charge modulation $\rho_1 \sin k_o x$ to excite the plasma. Here, ρ_1 is determined by requiring that Δt later $\rho_1 \sin k_o x$ will produce the usual velocity modulation $v_o(1 + 0.002 \cos k_o x)$, i.e., $\rho_1 = -0.002 v_o m k_o/q\,\Delta t$. Since aliases come in through grid quantities, it is hoped that such an excitation will create stronger alias modes, and, hence, the instability will show up earlier.

The results indicate that such an excitation does help observing the grid insta-

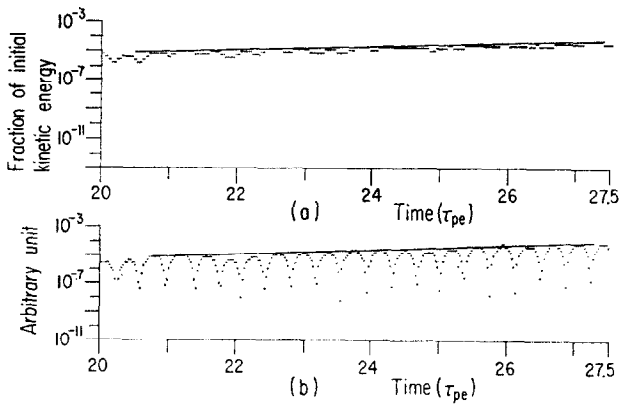

FIG. 5. Experiment of cold drifting beam with $v_o = 0.12\,\omega_{pe}\,\Delta x$ and two equal-spacing grid interlacing. The plasma was initially excited by charge modulation. Plots of (a) electric field energy and (b) square of the cosine component of the electric field vs time.

bility became the dominant mode at $t \cong 20\tau_{pe}$ instead of $25\tau_{pe}$ in the first experiment. Figure 5 shows the field-energy and cosine-square plots between $t = 20$ and $27.5\tau_{pe}$. The values of both ω_r and ω_i agree with the theoretical ones.

As far as verifying the theory for a Maxwellian plasma is concerned, we face the practical (economic) limit on the simulations. Since in a Maxwellian plasma the grid instabilities arise due to the scatterings between particles and alias waves, the loaded velocity distribution should be fine enough so that we have the required velocity spacing, $\Delta v \sim \omega_i/|k_p|$ in order that smooth distribution Vlasov theory may apply [9]. As stated in the theories, only even aliases contribute to the grid instabilities in a Maxwellian simulation plasma with two-time-step jiggled or interlaced grids. Hence, the smallest appropriate $|k_p|$ is $|k_2| = |k_o - 4\pi\Delta x^{-1}|$. Since generally $k_o \Delta x \lesssim 1$, we have $|k_2| \sim 4\pi\Delta x^{-1}$. Thus, $\Delta v_{max} \sim \omega_i \Delta x/4\pi$. For $v_{th} = 0.1\omega_{pe}\Delta x$ and $\omega_i \sim 10^{-3}\omega_{pe}$, we have $\Delta v_{max} \sim 10^{-3}v_{th}$. Thus, a very fine velocity representation is needed. Furthermore, to be a Vlasov plasma, we also require $n_0\lambda_{De} \gg 1$. The number of particles needed to satisfy both conditions as well as the computation time needed to observe these instabilities with small growth rates become rather impracticable for us. So far, we are content with the verifications given by the cold-beam case.

5. Experiment with Randomly Jiggled Grids

This experiment has the same parameters as those in other experiments. At each time step, the grids are placed randomly by a random number generator. Furthermore, in this experiment we had the run long enoug to observe the saturation of the nonphysical grid instability. The plasma was initially excited by the usual velocity modulation. Normalized-energy plots, cosine-square plot, and sine plot are shown in Fig. 6. From the field-energy plot, one can see that the instability began to show up around $t = 7\tau_{pe}$. The measured growth rate is about $0.10\omega_{pe}$ which is smaller than that with fixed grids but greater than that with two-time-step equal-spacing jiggled grids. The instability saturated about $t = 16\tau_{pe}$. During this period, the normalized field energy grew from $O(10^{-6})$ to $O(10^{-1})$. Again, there were odd–even jumpings, indicating the existence of a mode with $\omega_r \cong \pi/\Delta t$. That this high-frequency jiggled mode is the unstable mode can be clearly seen from the sine plot. Total and kinetic energy began to increase appreciably when the field energy reached $O(10^{-3})$ around $t = 12\tau_{pe}$. Around the saturation time, both energies increased by $O(10^{-1})$. Figure 7 shows the phase-space plots taken at four different time steps. As the instability grew, the initial-velocity modulation became appreciable around $t = 12\tau_{pe}$. There appeared to be higher spatial modes. This became obvious at $t = 14$ and $15\tau_{pe}$. The dominant higher harmonic is the 13th mode which corresponds to the $p = -1$ alias mode. As demonstrated by the

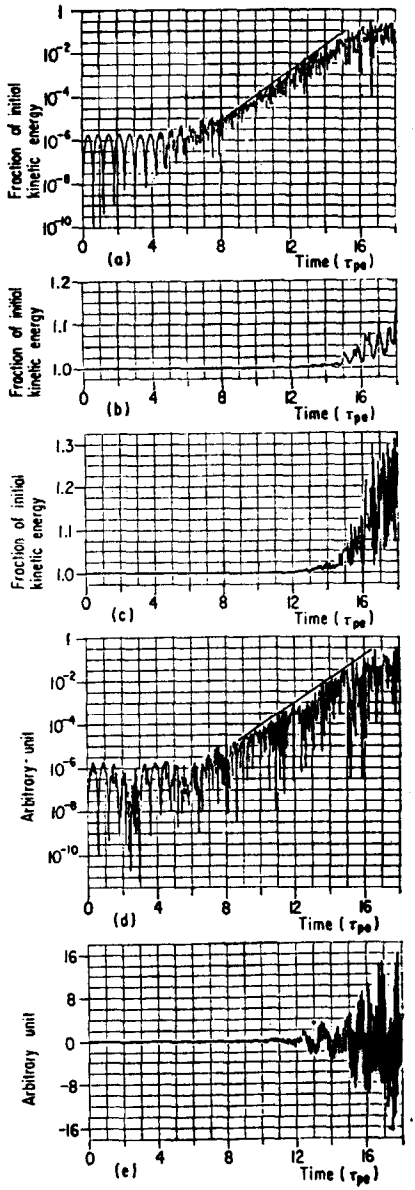

FIG. 6. Experiment of cold drifting beam with $v_o = 0.12\,\omega_{pe}\,\Delta x$ and random grid jiggling. Plots of (a) electric field energy, (b) kinetic energy, (c) total energy, (d) square of the cosine component of the electric field, and (e) the sine component of the electric field vs time.

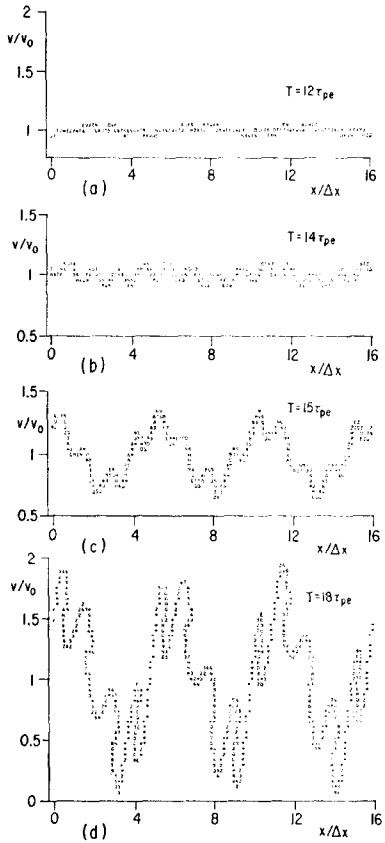

FIG. 7. Same experiment as in Fig. 6. Plots of the phase space at four different time steps.

phase-space plot at $t = 18\tau_{pe}$, the phase-space turbulence kept growing even after the instability had saturated.

Thus, random jiggling does not prove itself to be better than other ways of jiggling the grids.

6. Theory of Two-dimensional Simulations with Two Diagonally Jiggled or Interlaced Grids

As we have pointed out in Section 1, nonphysical grid properties may occur in 2- or 3-dimensional simulations due to the limit in the size of the random-access memory and, hence, the number of the grid points available. Therefore, it is

important to examine the properties of higher-dimensional simulation plasmas with jiggled or interlaced grids in order to check the possible benefits of grid jiggling or interlacing. No attempt is made here to develop a formal general theory. However, we have studied a simple but useful case, i.e., the grids are either diagonally jiggled or interlaced, and the qualitative results are presented in this section.

For the two-time-step diagonal-grid-jiggling case, the position of the jth grid, x_j, is in two dimensions (see Fig. 8):

$$\vec{x}_j = \begin{cases} (j\,\Delta x,\, j\,\Delta y) & \text{at even time steps,} \\ (j\,\Delta x + \tfrac{1}{2}\,\Delta x,\, j\,\Delta y + \tfrac{1}{2}\,\Delta y) & \text{at odd time steps.} \end{cases}$$

An equivalent point of view is that the grids are moving at a constant velocity in diagonal direction, $\vec{v}_{\text{grid}} = (\Delta x/2\,\Delta t,\, \Delta y/2\,\Delta t)$. Similar to the one-dimensional case, the aliases with alias number $\vec{p} = (p_x, p_y)$ feel a doppler shift $(\vec{p} \cdot \overleftrightarrow{k}_g) \cdot \vec{v}_{\text{grid}}$. Here in two dimensions,

$$\overleftrightarrow{k}_g = 2\pi \begin{pmatrix} \Delta x^{-1} & 0 \\ 0 & \Delta y^{-1} \end{pmatrix}.$$

Thus, by replacing ω in the dispersion relation for fixed grids [2, 3] by $\omega - \pi(p_x + p_y)/\Delta t$, we obtain the dispersion relation for two-time-step diagonally jiggled grids

$$\epsilon_{\text{diag } j,g}(\vec{k}, \omega) = 1 + \frac{\omega_{\text{pe}}^2}{K^2}\,\vec{\kappa} \cdot \Bigg\{ \sum_{\substack{\vec{p} \\ p_x+p_y=\text{even}}} |S(\vec{k}_{\vec{p}})|^2 \int dv \vec{f}_o{}' \,\frac{\Delta t}{2} \cot(\omega - \vec{k}_{\vec{p}} \cdot \vec{v})\,\frac{\Delta t}{2} - \sum_{\substack{\vec{p} \\ p_x+p_y=\text{odd}}} |S(\vec{k}_{\vec{p}})|^2 \int dv \vec{f}_o{}' \,\frac{\Delta t}{2} \tan(\omega - \vec{k}_{\vec{p}} \cdot \vec{v})\,\frac{\Delta t}{2} \Bigg\} = 0,$$

$$\text{Im}\,\omega \geqslant 0. \qquad (13)$$

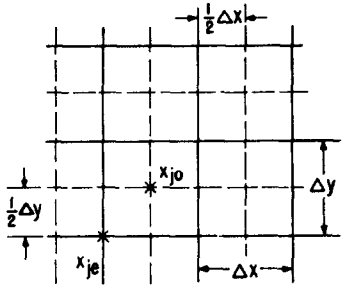

FIG. 8. Sketch to illustrate two-time-step diagonal grid jiggling in two dimensions.

Here, $\vec{k} = (k_x, k_y)$, $\vec{k}_{\vec{p}} = \vec{k} - \vec{p} \cdot \overleftrightarrow{k}_g = (k_x - 2\pi p_x/\Delta x,\ k_y - 2\pi p_y/\Delta y)$, and for CIC

$$S(\vec{k}) = \left(\frac{\sin \frac{1}{2}k_x \Delta x}{\frac{1}{2}k_x \Delta x}\right)^2 \left(\frac{\sin \frac{1}{2}k_y \Delta y}{\frac{1}{2}k_y \Delta y}\right)^2.$$

From previous experiences with the one-dimensional case, one can see from (13) that at low-frequency $|\omega \Delta t| \ll 1$, only aliases with $p_x + p_y =$ even number, e.g., $(1, -1)$, $(-1, 1)$, $(1, 1)$ and $(0, 2)$, contribute to the nonphysical grid effects. Those aliases with $p_x + p_y =$ odd numbers, e.g., $(1, 0)$, $(0, 1)$, $(-1, 0)$ and $(0, -1)$, are shifted to frequencies near the jiggling frequency, $\omega \cong \pi/\Delta t$. Furthermore, it is interesting to note that for $|k_x \Delta x|, |k_y \Delta_y| \lesssim 1$ and $p_x, p_y \neq 0$, we have

$$S(\vec{k}_{\vec{p}}) \simeq (k_x \Delta x)^2 (k_y \Delta y)^2/(4\pi^2 p_x p_y)^2 = O(\Delta x^2 \Delta y^2).$$

If, however, either p_x or p_y is zero, we then have

$$S(k) \simeq (k_x \Delta x/2\pi p_x)^2 \qquad \text{or} \qquad (k_y \Delta y/2\pi p_y)^2 = O(\Delta x^2 \text{ or } \Delta y^2).$$

Therefore, for $|\omega \Delta t| \ll 1$ and $|k_x \Delta x|, |k_y \Delta y| \lesssim 1$, the most troublesome aliases are $(0, 2)$, $(2, 0)$, $(0, -2)$, and $(-2, 0)$. The nonphysical effects of aliases $(-1, 1)$, $(1, -1)$, $(1, 1)$, and $(-1, -1)$ have been greatly reduced, to fourth order in Δx, Δy by the effective shaping factor S. That is, at low frequencies, the grid effects are effectively reduced to those of a four-times-finer grid, with only twice as much computing, which is rather encouraging. As in one-dimensional case, we then expect the growth rate of the grid instability to be greatly reduced at low frequencies. Also, we expect that, depending on the velocity distribution, those shifted aliases ($p_x + p_y =$ odd numbers) may or may not give rise to grid instabilities.

With two diagonally interlaced grids, as might be expected, aliases with $(p_x + p_y) =$ odd numbers are completely eliminated and only aliases with $(p_x + p_y) =$ even numbers contribute to the nonphysical grid properties of the simulation plasmas. As in the jiggling case, the effective shaping factor further reduces the effects of aliases with $p_x, p_y \neq 0$, and, therefore, great reduction in the grid effects is expected.

7. Conclusions and Discussion

In the previous sections we have theoretically analyzed and tried in simulations the ideas of reducing the nonphysical grid effects by jiggling or interlacing the grids. General dispersion relations are derived and evaluated numerically for some specific cases. It is shown that grid jiggling shifts certain groups of aliases to high frequencies of order Δt^{-1}. For example, in the three-time-step equal-spacing

jiggling case, aliases with alias number $p \neq 3K$ (K an integer) are shifted to frequencies $2\pi/3\,\Delta t$ or $4\pi/3\,\Delta t$. For a Maxwellian plasma and over the ranges of the parameters investigated, these high-frequency modes are stable, and, therefore, grid instabilities are caused by only even aliases at low frequencies. The growth rates are greatly reduced. Numerical evaluations of the two-time-step equal-spacing dispersion relation indicate that for a cold drifting electron beam, these high-frequency modes are unstable. The high-frequency modes can be completely eliminated by interlacing the grids at each time step. With two equal-spacing interlaced grids, the odd aliases are eliminated and only even aliases contribute, which greatly reduces nonphysical grid effects. Simulations have been done and the results are in excellent agreement with the theories. Experimental results with randomly jiggled grids suggest that random jiggling may not be better than other grid-jiggling methods.

We also have studied theoretically the case of two-dimensional simulations with diagonally jiggled or interlaced grids. The qualitative pictures are similar to those in one dimension, and within $O(\Delta x^2\,\Delta y^2)$, one reduces the grid effects to those of a grid with *four* times as many grid points by doing only *twice* as much computing.

It thus appears that while grid jiggling (with no increase in computation time) may or may not reduce the nonphysical grid effects due to coarse grids, grid interlacing is rather promising. The price one pays for this improvement is that the particles have to be processed more than once.

APPENDIX: General Theory of Grid Jiggling

Theories of the two- and three-time-step grid jigglings are analyzed here to illustrate the approaches to more general cases. In the case of the two-time-step jiggling, the position of the jth grid, x_j, assumes two different values for odd and even time steps. That is, referring to Fig. 1(a),

$$x_j = \begin{cases} j\,\Delta x & \text{at even time steps,} \\ (j+\alpha)\,\Delta x, \quad 0 \leqslant \alpha \leqslant 1 & \text{at odd time steps.} \end{cases}$$

All physical quantities are then separated into two parts. One is defined only at even time steps and the other only at odd time steps. Subscripts, e and o, are used to denote these two parts. For example:

first-order particle density: $n(x, t) = n_e(x, t) + n_o(x, t)$,

grid charge density: $\rho(x, t) = \rho_e(x, t) + \rho_o(x, t)$,

where, e.g., $n_e(x, t) = \sum_\ell n(x, t)\,\delta(t - 2\ell\,\Delta t)$,

$$n_o(x, t) = \sum_\ell n(x, t)\,\delta[t - (2\ell + 1)\,\Delta t].$$

As done in actual simulations, a relation between ρ and n can be obtained, which is

$$\rho_e(k, \omega) = q \sum_{p=-\infty}^{\infty} S(k_p)\, n_e(k_p, \omega), \qquad \text{Im } \omega \geqslant 0; \tag{A.1}$$

$$\rho_o(k, \omega) = q \sum_{p=-\infty}^{\infty} S(k_p)\, e^{ip2\pi\alpha} n_o(k_p, \omega), \qquad \text{Im } \omega \geqslant 0. \tag{A.2}$$

One sees immediately from (A.2) that jiggling grids causes phase shifts in the aliases.

To obtain a linear dispersion relation, the simulation plasma is assumed to be Vlasov and particles are assumed to have deviated little from their unperturbed orbits. Particle density then is related to the initial velocity distribution, zero-order position, and first-order position in the following way:

$$n_{e,o}(x_r{}^0, t_r) = -n_0 \int dv^0 f_o(v^0) \frac{\partial}{\partial x_r{}^0} x_r{}^1(v^0, t_r). \tag{A.3}$$

Superscripts denote orders of quantities, $t_r = r\,\Delta t$, and that the subscript is "e" or "o" depends on whether r is even or odd. In normal simulation codes,

$$x_r{}^1 = \frac{\Delta t^2}{m} \sum_{r'=0}^{r-1} (r - r')\, F(x_{r'}^0, t_{r'}). \tag{A.4}$$

Here, F is the force on the particle and is evaluated along its unperturbed orbit. In simulations, force and grid charge are related through Poisson's equation, force sharing, and particle size, i.e.,

$$F_{e,o}(k, \omega) = \frac{q}{\epsilon_o} S(-k) \frac{[-i\kappa(k)]}{K^2(k)} \rho_{e,o}(k, \omega). \tag{A.5}$$

Combining (A.3)–(A.5), one obtains after some algebra

$$n_e(k, \omega) = \frac{n_0 q}{m\epsilon_o} S(-k) \frac{\kappa(k)}{K^2(k)} [\psi_2(k,,\omega)\, \rho_e(k, \omega) + \psi_1(k, \omega)\, \rho_o(k, \omega)], \tag{A.6}$$

$$n_o(k, \omega) = \frac{n_0 q}{m\epsilon_o} S(-k) \frac{\kappa}{K^2} [\psi_1 \rho_e + \psi_2 \rho_o], \tag{A.7}$$

where with $\omega_d = \omega - kv^0$,

$$\psi_1(k, \omega) = \int dv^0 f_o'(v^0) \frac{e^{-i\omega_d \Delta t} i\,\Delta t}{e^{-2i\omega_d \Delta t} - 1}, \tag{A.8}$$

$$\psi_2(k, \omega) = \int dv^0 f_o'(v^0) \frac{i\,\Delta t}{e^{-2i\omega_d \Delta t} - 1}. \tag{A.9}$$

Also, one has

$$\rho_e(k_p, \omega) = \rho_e(k, \omega), \qquad \rho_o(k_p, \omega) = e^{i2\pi p\alpha}\rho_o(k, \omega). \tag{A.10}$$

Substituting (A.6), (A.7), and (A.10) into (A.1) and (A.2), one finally arrives at the following relations:

$$\left[1 - \omega_{pe}^2 \frac{\kappa}{K^2} \sum_p |S(k_p)|^2 \psi_2(k_p, \omega)\right] \rho_e(k, \omega)$$

$$+ \left[-\omega_{pe}^2 \frac{\kappa}{K^2} \sum_p |S(k_p)|^2 e^{i2\pi p\alpha} \psi_1(k_p, \omega)\right] \rho_o(k, \omega) = 0, \tag{A.11}$$

$$\left[-\omega_{pe}^2 \frac{\kappa}{K^2} \sum_p |S(k_p)|^2 e^{i2\pi p\alpha} \psi_1(k_p, \omega)\right] \rho_e(k, \omega)$$

$$+ \left[1 - \omega_{pe}^2 \frac{\kappa}{K^2} \sum_p |S(k_p)|^2 \psi_2(k_p, \omega)\right] \rho_o(k, \omega) = 0. \tag{A.12}$$

A dispersion relation for any α then can be obtained from (A.11) and (A.12) by letting the 2×2 determinant vanish. The results for arbitrary α's can be rather complicated. However, one can show with some algebra that for $\alpha = 0$ and $1/2$, the dispersion relation can be reduced to (1) and (3), respectively.

Theory of the three-time-step grid jiggling develops very similarly to the two-time-step case. The position of the jth grid, x_j, now assumes three different values for three consecutive time steps, that is,

$$x_j(t) = \begin{cases} j\,\Delta x & \text{for } t = 3q\,\Delta t, \\ j\,\Delta x + \alpha\,\Delta x & \text{for } t = (3q+1)\,\Delta t, \\ j\,\Delta x + \beta\,\Delta x & \text{for } t = (3q+2)\,\Delta t, \end{cases} \qquad \begin{array}{l} q = \text{integers}, \\ 0 \leqslant \alpha, \beta \leqslant 1. \end{array}$$

Physical quantities, then, are divided into three parts corresponding to the three different positions, e.g., $n(x, t) = n_1(x, t) + n_2(x, t) + n_3(x, t)$;

here

$$n_1(x, t) = \sum_q n(x, t)\, \delta(t - 3q\,\Delta t),$$

$$n_2(x, t) = \sum_q n(x, t)\, \delta[t - (3q+1)\,\Delta t],$$

$$n_3(x, t) = \sum_q n(x, t)\, \delta[t - (3q+2)\,\Delta t].$$

The rest of the procedures are just the same as those in the two-time-step jiggling case. Equations corresponding to (A.11) and (A.12) are

$$\left[1 - \omega_{pe}^2 \frac{\kappa}{K^2} \sum_p |S(k_p)|^2 G_1(k_p, \omega)\right] \rho_1(k, \omega)$$
$$- \left[\omega_{pe}^2 \frac{\kappa}{K^2} \sum_p |S(k_p)|^2 G_2(k_p, \omega) e^{i2\pi p\alpha}\right] \rho_2(k, \omega)$$
$$- \left[\omega_{pe}^2 \frac{\kappa}{K^2} \sum_p |S(k_p)|^2 G_3(k_p, \omega) e^{i2\pi p\beta}\right] \rho_3(k, \omega) = 0, \tag{A.13}$$

$$- \left[\omega_{pe}^2 \frac{\kappa}{K^2} \sum_p |S(k_p)|^2 G_3(k_p, \omega) e^{i2\pi p\alpha}\right] \rho_1(k, \omega)$$
$$+ \left[1 - \omega_{pe}^2 \frac{\kappa}{K^2} \sum_p |S(k_p)|^2 G_1(k_p, \omega)\right] \rho_2(k, \omega)$$
$$- \left[\omega_{pe}^2 \frac{\kappa}{K^2} \sum_p |S(k_p, \omega)|^2 G_2(k_p, \omega) e^{i2\pi p(\beta-\alpha)}\right] \rho_3(k, \omega) = 0, \tag{A.14}$$

$$- \left[\omega_{pe}^2 \frac{\kappa}{K^2} \sum_p |S(k_p)|^2 G_2(k_p, \omega) e^{i2\pi p\beta}\right] \rho_1(k, \omega)$$
$$- \left[\omega_{pe}^2 \frac{\kappa}{K^2} \sum_p |S(k_p)|^2 G_3(k_p, \omega) e^{i2\pi p(\beta-\alpha)}\right] \rho_2(k, \omega)$$
$$+ \left[1 - \omega_{pe}^2 \frac{\kappa}{K^2} \sum_p |S(k_p)|^2 G_1(k_p, \omega)\right] \rho_3(k, \omega) = 0; \tag{A.15}$$

and here with $\omega_d = \omega - kv$,

$$G_1(k, \omega) = \int dv f_o' \frac{i\,\Delta t}{e^{-3i\omega_d \Delta t} - 1}, \tag{A.16}$$

$$G_2(k, \omega) = \int \frac{dv f_o' i\,\Delta t\, e^{-i\omega_d \Delta t}}{e^{-3i\omega_d \Delta t} - 1}, \tag{A.17}$$

$$G_3(k, \omega) = \int \frac{dv f_o' i\,\Delta t\, e^{-2i\omega_d \Delta t}}{e^{-3i\omega_d \Delta t} - 1}. \tag{A.18}$$

Again, a generally rather complicated dispersion relation for any α and β can be obtained from (A.13)–(A.15) by letting the 3×3 determinant vanish. For $\alpha = \beta = 0$, however, the dispersion reduces to (1) as it should. Also, for $\alpha = 1/3$ and $\beta = 2/3$, the dispersion relation can be shown with some algebra to reduce to (7).

In fact, one can write down the dispersion relation for the N-time-step case. Assuming that x_j at the ℓth time step such that $\ell = KN + s$ (K = integers; $s = 0, 1, \ldots, N-1$) is

$$x_j(\ell\,\Delta t) = (j + \alpha_s)\,\Delta x, \qquad 0 \leqslant \alpha_s \leqslant 1,$$

then the dispersion relation is

$$\det |\,\overleftrightarrow{I} - \overleftrightarrow{A}\,| = 0. \tag{A.19}$$

Here $\overleftrightarrow{I}$ is the unit matrix and the elements of $\overleftrightarrow{A}$ are

$$A_{mn} = \sum_p W_{N+n-m} e[p(\alpha_{n-1} - \alpha_{m-1})], \qquad m, n = 1, \ldots, N, \tag{A.20}$$

where with $\omega_{dp} = \omega - k_p v$,

$$W_L(k_p, \omega) = \omega_{pe}^2 \frac{\kappa}{K^2} |\,S(k_p)|^2 \int dv f_0' \frac{i\,\Delta t\, e^{-iL\omega_{dp}\Delta t}}{e^{-iN\omega_{dp}\Delta t} - 1}. \tag{A.21}$$

$$W_{N+L} = W_L,$$

and

$$e(x) \equiv e^{i2\pi x}. \tag{A.22}$$

For $\alpha_0 = \alpha_2 = \cdots = \alpha_{N-1} = 0$, (A.19) can be reduced to the dispersion relation for fixed grids, (1). Also, (2) can be obtained from (A.19) by letting $\alpha_s = s/N$ for $s = 0, 2, \ldots, N-1$.

As an example of applications of this otherwise rather complicated dispersion relation, let us examine a case which may be of interest to *two-dimensional* simulations with jiggled grids. Assuming in two dimensions the jth grid takes on the following positions (referring to Fig. A.1): $(j\,\Delta x, j\,\Delta y)$, $(j\,\Delta x, j\,\Delta y + (1/2)\,\Delta y)$, $(j\,\Delta x + (1/2)\,\Delta x, j\,\Delta y + (1/2)\,\Delta y)$, and $(j\,\Delta x + (1/2)\,\Delta x, j\,\Delta y)$, then for waves propagating *only* in the $\hat{x}$ direction, this two-dimensional case reduces to the one-dimensional case with $N = 4$, $\alpha_0 = 0$, $\alpha_1 = 0$, $\alpha_2 = 1/2$, and $\alpha_3 = 1/2$. Substituting the values of N and the α's into (A.19), we obtain after some algebra the following dispersion relation:

$$\epsilon(k, \omega) = \epsilon_e(k, \omega)\,\epsilon_e(k, \omega + (\pi/\Delta t)) - \epsilon_0^2(k, \omega) = 0, \qquad \operatorname{Im}\omega \geqslant 0, \tag{A.23}$$

where

$$\epsilon_e(k, \omega) = 1 + \omega_{pe}^2 \frac{\kappa}{K^2}\left[\sum_{p:\text{even}} |\,S(k_p)|^2 \int dv f_0' \frac{\Delta t}{2} \cot(\omega - k_p v) \frac{\Delta t}{2}\right.$$

$$\left. - \sum_{p:\text{odd}} |\,S(k_p)|^2 \int dv f_0' \frac{\Delta t}{2} \tan(\omega - k_p v)\,\Delta t\right] \tag{A.24}$$

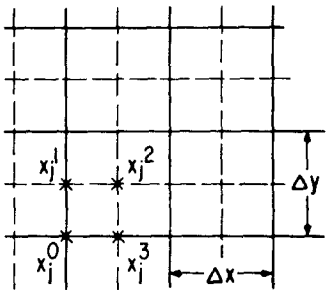

FIG. A1. A sketch of jiggled grid positions in two dimensions.

and

$$\epsilon_o(k, \omega) = \omega_{pe}^2 \frac{\kappa}{K^2} \sum_{p:\text{odd}} |S(k_p)|^2 \int dv f_o' \frac{\Delta t}{2} \sec(\omega - k_p v)\, \Delta t. \quad \text{(A.25)}$$

For $|(\omega - k_p v)\, \Delta t| \ll 1$, (A.23) approximates as

$$\epsilon(k, \omega) \simeq 1 + \omega_{pe}^2 \frac{\kappa}{K^2} \sum_{p:\text{even}} |S(k_p)|^2 \int dv f_o' \frac{1}{\omega - k_p v} + O[(\omega_{pe}\, \Delta t)^2] \simeq 0,$$

$$\text{Im}\, \omega \geqslant 0. \quad \text{(A.26)}$$

For $\omega = \omega' + \pi/\Delta t$ such that $|(\omega' - k_p v)\, \Delta t| \ll 1$, we obtain a result similar to (A.26) except ω is replaced by ω' here. However, for $\omega = \omega'' \pm \pi/2\, \Delta t$ and $|(\omega'' - k_p v)\, \Delta t| \ll 1$, the results are different. In this case, (A.23) approximates as

$$\epsilon(k, \omega) = \epsilon(k, \omega'' \pm \pi/2\, \Delta t) \simeq 1 + \omega_{pe}^2 \frac{\kappa}{K^2} \sum_{p:\text{odd}} |S(k_p)|^2 \int dv f_o' \frac{1}{\omega'' - k_p v}$$

$$+ O[(\omega_{pe}\, \Delta t)^2] \simeq 0, \qquad \text{Im}\, \omega \geqslant 0. \quad \text{(A.27)}$$

Thus, for $|\omega\, \Delta t| \ll 1$ and $\omega\, \Delta t \cong \pi$, even aliases contribute dominantly to nonphysical properties of the simulation plasmas. Therefore, if the simulation plasma is nonphysically unstable at low frequencies, then in this case it is also unstable at $\omega \sim \pi/\Delta t$. For $\omega\, \Delta t \simeq \pi/2$, however, the odd aliases make the dominant contributions and additional nonphysical instabilities can occur. For example, as we have shown earlier that a Maxwellian plasma is stable against odd aliases but nonphysically unstable if the even aliases are present. Thus, it is expected that the plasma will have reduced grid instabilities at $|\omega\, \Delta t| \ll 1$ and $\omega\, \Delta t \simeq \pi$. With a cold drifting beam, however, strongest grid instabilities will occur at $\omega\, \Delta t \simeq \pm\pi/2$. Therefore, so far as waves propagating only in the $\hat{x}$ direction are concerned, this grid-jiggling pattern is less desirable than the $(j\, \Delta x, j\, \Delta y)$, $(j\, \Delta x + (1/2)\, \Delta x, j\, \Delta y)$

or $(j\,\Delta x, j\,\Delta y)$, $(j\,\Delta x + (1/2)\,\Delta x, \Delta y)$ jiggling pattern which reduces to the two-time-step equal-spacing jiggling in one dimension and, therefore, has reduced grid instabilities only at $|\,\omega\,\Delta t\,| \ll 1$.

References

1. E. L. Lindman, *J. Computational Phys.* **5** (1970), 13.
2. A. B. Langdon, *J. Computational Phys.* **6** (1970), 247.
3. A. B. Langdon, in Proceedings of the Fourth Annual Conference on Numerical Simulation of Plasmas, (1970). U.S. Govt. Printing Office, Washington, C.D. 20402, Stock No. 0851 0059.
4. R. W. Hockney, *J. Computational Phys.* **8** (1971), 19.
5. H. Okuda, *J. Computational Phys.* **10** (1972), 475.
6. J. P. Boris, Matt-769, Princeton Plasma Physics Laboratory (1970). Also, A. B. Langdon and J. P. Boris, to be published in *J. Computational Phys.*
7. C. K. Birdsall and D. Fuss, *J. Computational Phys.* **3** (1969), 494.
8. A. B. Langdon, *J. Computational Phys.*, in press.
9. J. M. Dawson, *Phys. Rev.* **118** (1960), 381.